

# Strong asymmetry of the electron-loss-to-continuum cusp of multielectron $U^{28+}$ projectiles in near-relativistic collisions with gaseous targets

P.-M. Hillenbrand,<sup>1,\*</sup> S. Hagmann,<sup>1</sup> J. M. Monti,<sup>2</sup> R. D. Rivarola,<sup>2</sup> K.-H. Blumenhagen,<sup>1,3,4</sup> C. Brandau,<sup>1,5</sup> W. Chen,<sup>1,†</sup> R. D. DuBois,<sup>6</sup> A. Gumberidge,<sup>1</sup> D. L. Guo,<sup>7</sup> M. Lestinsky,<sup>1</sup> Yu. A. Litvinov,<sup>1</sup> A. Müller,<sup>8</sup> S. Schippers,<sup>5</sup> U. Spillmann,<sup>1</sup> S. Trotsenko,<sup>1,3</sup> G. Weber,<sup>3</sup> and Th. Stöhlker<sup>1,3,4</sup>

<sup>1</sup>*GSI Helmholtzzentrum für Schwerionenforschung, 64291 Darmstadt, Germany*

<sup>2</sup>*Instituto de Física Rosario, CONICET and Facultad de Ciencias Exactas, Ingeniería y Agrimensura, Universidad Nacional de Rosario, 2000 Rosario, Argentina*

<sup>3</sup>*Helmholtz-Institut Jena, 07743 Jena, Germany*

<sup>4</sup>*Institut für Optik und Quantenelektronik, Friedrich-Schiller-Universität Jena, 07743 Jena, Germany*

<sup>5</sup>*I. Physikalisches Institut, Justus-Liebig-Universität Giessen, 35392 Giessen, Germany*

<sup>6</sup>*Missouri University of Science and Technology, Rolla, Missouri 65409, USA*

<sup>7</sup>*Institute of Modern Physics, Chinese Academy of Sciences, Lanzhou 730000, China*

<sup>8</sup>*Institut für Atom- und Molekülphysik, Justus-Liebig-Universität Giessen, 35392 Giessen, Germany*

(Received 2 March 2016; published 25 April 2016)

The process of electron-loss to the continuum (ELC) has been studied for the collision systems  $U^{28+} + H_2$  at a collision energy of 50 MeV/u,  $U^{28+} + N_2$  at 30 MeV/u, and  $U^{28+} + Xe$  at 50 MeV/u. The energy distributions of cusp electrons emitted at an angle of  $0^\circ$  with respect to the projectile beam were measured using a magnetic forward-angle electron spectrometer. For these collision systems far from equilibrium charge state, a significantly asymmetric cusp shape is observed. The experimental results are compared to calculations based on first-order perturbation theory, which predict an almost symmetric cusp shape. Some possible reasons for this discrepancy are discussed.

DOI: [10.1103/PhysRevA.93.042709](https://doi.org/10.1103/PhysRevA.93.042709)

## I. INTRODUCTION

Despite its long history of research, the process of projectile ionization during the collision with a target atom is not fully understood [1–5]. For projectiles of high atomic number  $Z_p$ , theoretical predictions are particularly challenging [4]. Experimental total ionization cross sections of heavy few-electron projectiles in effective charge-states  $Z_p^{\text{eff}} \approx Z_p$  have meanwhile been reproduced by an *ab initio* theory even for higher target atomic numbers  $Z_t$  [6]. In comparison to total cross sections, experimental data of differential cross sections provide a considerably more stringent test to *ab initio* theories [1,7–9]. For projectile ionization in fast ion-atom collisions, differential cross sections of the emitted electrons are strongly enhanced in the forward direction. Corresponding spectra can be accessed by measuring the electron cusp, i.e., the energy distribution of electrons emitted under an angle of  $\vartheta_e \approx 0^\circ$  with respect to the projectile beam and having a velocity similar to the projectile velocity [2,10–18]. Deviations from a symmetric cusp shape measured in the laboratory frame-of-reference can be traced back to an anisotropic electron emission in the projectile frame [19–22].

For the case of low atomic numbers of the target atom,  $Z_t \ll Z_p^{\text{eff}}$ , and comparably high collision velocities (in atomic units),  $v_p \gg Z_t$ , the projectile is dominantly ionized through a weak perturbation, characterized by a comparably short interaction time [4,6]. Under these conditions, the ionization process can be treated in first-order perturbation theory, where the double-

differential cross section of the electron distribution scales as  $Z_t^2$  and its shape is independent of  $Z_t$ . For such a case of a heavy few-electron projectile,  $U^{88+}(1s^22s^2)$ , ionized by a nitrogen target, an agreement of experimental and theoretical differential cross sections of the electron-loss-to-continuum cusp has recently been reported [19]. However, an electron cusp shape that varies with  $Z_t$  is an indication for a process, where the interaction is not reliably described as first-order perturbation, as will be shown in this paper for collisions of  $U^{28+}$  projectiles on  $H_2$ ,  $N_2$ , and  $Xe$  targets.

A significant increase in complexity is introduced, when heavy medium-charged multielectron projectiles are used, e.g., with  $Z_p^{\text{eff}} \approx Z_p/2$ . Not only does the theoretical description require bound-state wave functions of the multielectron projectile. But also, due to low binding energies of the least-bound projectile electrons, the collision velocity may be far above charge-state equilibrium. For these collision systems, large impact parameters may become dominant, such that the screening of the target nucleus by the target electrons is relevant.

Experimental total cross sections for multielectron projectile ionization [23–26] have been partially reproduced by various theories [27–29]. A strong contribution of multiple ionization was observed in Refs. [30–35]. However, experimental data for corresponding differential ionization cross sections of dressed heavy projectiles did not exceed the level of proof-of-principle [13–17]. Furthermore, an *ab initio* theory predicting differential and total cross sections for the ionization of multielectron heavy projectiles in ion-atom collisions has not been developed up to now.

Besides the basic interest in understanding one of the fundamental atomic collision processes, projectile ionization in ion-atom collisions has a significant relevance for the beam physics of heavy-ion accelerators. The beam intensity of

\*p.m.hillenbrand@gsi.de

†Present address: Institute of High Energy Physics, Chinese Academy of Science, Dongguan 523803, China.

heavy-ion synchrotrons is ultimately limited by space-charge effects. These effects can only be reduced by decreasing the charge state of the accelerated ions at the expense of an increased magnetic rigidity required for the same ion beam energy. Here, the ionization of heavy medium-charged ions by atoms of the residual gas plays a crucial role, since charge-exchanged ions are lost during the acceleration process. In addition, ion-beam lifetimes in synchrotrons are limited by the effect of dynamic vacuum [36,37]. For instance, in the heavy-ion accelerator chain of FAIR,  $U^{28+}$ -ions are planned to be accelerated consecutively in the synchrotrons SIS18 and SIS100 from an energy of 11.4 MeV/u to 2.7 GeV/u [38].

This motivates the current study of differential cross sections for the ionization of  $U^{28+}([Kr]4d^{10}4f^{14}5s^25p^2)$  in collisions with the three gaseous neutral targets. Measured and calculated energy spectra of cusp electrons for the collision systems  $U^{28+} + H_2$  at 50 MeV/u,  $U^{28+} + N_2$  at 30 MeV/u, and  $U^{28+} + Xe$  at 50 MeV/u are presented. Unprecedentedly clean experimental conditions were facilitated by using the magnetic forward-angle electron spectrometer [19–22] installed in the experimental storage ring ESR of the heavy-ion accelerator facility GSI Helmholtzzentrum für Schwerionenforschung. The measured spectra are compared with theoretical calculations based on first-order perturbation theory applying relativistic wave functions for the initial bound states of the heavy multielectron projectile, and the observed discrepancies between experiment and theory are discussed. These inconsistencies may also question the theoretical models used for the calculation of ion-beam lifetimes in heavy-ion accelerators.

The paper is organized as follows: In Sec. II the experimental setup is briefly described, in Sec. III the data analysis is explained, in Sec. IV the concept of the theoretical calculations is given, and in Sec. V the experimental results are discussed in comparison with theory.

## II. EXPERIMENT

The experiment was conducted at the heavy-ion accelerator facility GSI Helmholtzzentrum für Schwerionenforschung. The uranium ions were stripped to their final charge state  $28+$  within the linear accelerator UNILAC at an energy of 1.4 MeV/u, accelerated in the synchrotron SIS18 to 30 or 50 MeV/u, and injected into the heavy-ion storage ring ESR. In the ESR, electron cooling was applied, and the  $U^{28+}$  projectile ion beam was intersected with a supersonic gas-jet of  $H_2$ ,  $N_2$ , or  $Xe$ . The average number of  $U^{28+}$  projectile ions circulating in the ring was about  $3 \times 10^6$ . The average area density of target atoms was about  $3 \times 10^{10} \text{ cm}^{-2}$  for H,  $8 \times 10^{10} \text{ cm}^{-2}$  for N, and  $2 \times 10^9 \text{ cm}^{-2}$  for Xe.

The energy distributions of electrons emitted from the interaction point into the forward direction were measured with a magnetic electron spectrometer by counting the observed electrons as a function of the magnetic fields applied to the spectrometer. The corresponding momentum analysis was performed by two consecutive  $60^\circ$ -dipole magnets. A magnetic iron-free quadrupole triplet between the dipole magnets provided the increased angular acceptance by focusing the traversing electrons. The angular acceptance with respect to the projectile beam was given by  $\vartheta_e = 0^\circ - \vartheta_{\max} = 0^\circ - 2.4^\circ$

in the polar direction and by the whole azimuthal angle,  $\varphi_e = 0^\circ - 360^\circ$ . The relative momentum acceptance resulting from the electron optics was  $\Delta p_e/p_e = 0.02$ . The field of the dipole magnets was measured with hall probes, determining the relative momentum scale of the measured electron spectra. The electron detection was facilitated by a stack of two microchannel plates in chevron configuration and a position-sensitive hexagonal delay-line anode. The position information of the detector was used as a diagnostic tool to ensure a correct scaling of the electron optical elements throughout the measured energy range. In the evaluation of the cross sections only the count rate of the detector was used. A detailed description of the experimental setup is given in Ref. [19].

Since the ESR is optimized for the storage and study of heavy few-electron ions, the use of heavy medium-charged ions like  $U^{28+}$  at the ESR is characterized by the following constraints: (i) The upper limit for the projectile energy accessible at the ESR is given by the maximum magnetic rigidity of 10 Tm, which corresponds to about 60 MeV/u for  $U^{28+}$ . (ii) The lower limit for the projectile energy at about 10 MeV/u is given by the short lifetime of the stored ions at low projectile energies due to large cross sections for ionization and recombination in the residual gas [25,29,39]. (iii) The lifetime of the  $U^{28+}$  ion beam is additionally reduced by enhanced recombination losses during electron cooling [40,41]. (iv) The relatively large change in the mass-to-charge ratio when ionizing to  $U^{29+}$  or recombining to  $U^{27+}$  made it impossible to detect the charge-exchanged projectiles by the available particle detectors installed in the dispersive sections of the ESR, such that no coincidence measurement of the ionized projectile with the emitted electron was possible in the applied experimental configuration. (v) Due to the low projectile velocity and the low charge state, the signal induced in the beam current transformer is relatively weak, such that only a significant increase of the beam intensity for  $U^{28+}$  ions provided by the UNILAC [42] and SIS18 within the last few years enabled a reliable determination of the ion beam intensity in the ESR.

These arguments motivated the choice of the projectile energies studied in this paper. The projectile energy was determined from the voltage applied to the electron cooler. The chosen energy of 30 MeV/u corresponds to a projectile velocity in units of the speed of light  $\beta = 0.2478$ , or in atomic units  $v_p = 33.96 \text{ a.u.}$ , a Lorentz factor of  $\gamma = 1.032$ , and an electron cusp energy of  $E_0 = 16.46 \text{ keV}$ . The energy of 50 MeV/u corresponds to  $\beta = 0.3151$ ,  $v_p = 43.18 \text{ a.u.}$ ,  $\gamma = 1.054$ , and  $E_0 = 27.43 \text{ keV}$ .

## III. DATA ANALYSIS

The experimental cross sections were evaluated from the background-corrected number of electrons  $N_e$  observed in the spectrometer through

$$\frac{d^2\sigma}{dE_e d\Omega_e} \Big|_{\vartheta_e=0^\circ} = \frac{N_e}{L_{\text{int}}} \frac{1}{\epsilon_e \Delta\Omega_e} \frac{E_e + m_e c^2}{E_e^2 + 2E_e m_e c^2} \frac{1}{\Delta p_e/p_e}. \quad (1)$$

Here, the electron detection efficiency is  $\epsilon_e$ , the observation solid angle  $\Delta\Omega_e \approx \pi \vartheta_{\max}^2$ , and the relative momentum acceptance  $\Delta p_e/p_e$ . The energy factor with the electron rest energy  $m_e c^2$  includes the transformation of momentum-

differential to energy-differential cross sections  $dp_e/dE_e$  and the dispersion correction  $1/p_e(\Delta p_e/p_e)$ , i.e., the increasing absolute momentum acceptance with increasing momentum. The integrated luminosity  $L_{\text{int}}$  in units of  $\text{barn}^{-1}$  was determined by integration of the product of ion beam current  $I_{\text{ion}}(t)$  and target area density  $n_{\text{target}}(t)$  over the measurement time  $t$ ,

$$L_{\text{int}} = \int \frac{I_{\text{ion}}(t) n_{\text{target}}(t)}{Z_p^{\text{eff}} e} dt, \quad (2)$$

with  $Z_p^{\text{eff}} e = 28e$  being the projectile charge. The ion beam current was measured by the beam current transformer. The target area density was determined from the pressure increase in the target dump measured by four calibrated vacuum gauges [26,43]. Due to uncertainties in the determination of the absolute scale of  $L_{\text{int}}$  and the unknown electron detection efficiency  $\epsilon_e$ , the measured data are only relative cross sections, which were normalized to the absolute scale of the results of the theoretical calculations. The error bars include a quadratic summation of the statistical error and the estimated relative systematic error. The dominant contribution is the relative error in the determination of  $L_{\text{int}}$ , which is conservatively assumed to be 20%. Please note that the complementary study of absolute total projectile ionization cross sections for the same collision systems is published in Ref. [26].

The energy scale of the presented experimental data was derived from the relative momentum scale, which is proportional to the values of the magnetic fields of the spectrometer dipoles measured with hall probes. The electron momentum was thus determined on a relative scale with a precision better than  $10^{-3}$ . The absolute energy scale was calibrated through the well-known fact that the maximum of the electron distribution is at the electron cusp energy  $E_0$  [44], which in turn is identical to the (space-charge corrected) kinetic energy of electrons in the electron cooler.

#### IV. THEORY

The theoretical calculations were performed based on the distorted wave models published by Monti *et al.* [45,46]. These models were devised to study ionization of multielectron atoms and molecules by partially dressed ion impact and later extended to study projectile electron loss and simultaneous target-projectile ionization [47]. More recently (see Ref. [21]) relativistic kinematics were implemented in order to take into account high collision velocities.

In the present work we only focus on the projectile ionization during collisions with a neutral target atom. The molecular character of the  $\text{H}_2$  and the  $\text{N}_2$  target is neglected, since the respective molecular binding energies are small compared to the collision energies, and all cross sections are given per target atom.

The presently studied collision systems are far from their equilibrium charge states. Therefore, the binding energies  $E_p^b$  of the outer projectile electrons, which dominate the electron spectra, are comparatively low (cf. Table I). Consequently, the ionization of the projectile by the target atom occurs at comparably large impact parameters. At these large impact parameters, the Coulomb field of the target nucleus is partially screened by the electrons

TABLE I. Orbital binding energies,  $E_p^b$ , for the individual subshells of  $\text{U}^{28+}$ : The values based on relativistic Dirac-Fock (DF) theory are taken from Ref. [48], and the values based on relativistic multiconfiguration Dirac-Fock (MCDF) theory are calculated using GRASP92 [49]. The MCDF values are used in this work.

Subshell of $\text{U}^{28+}$	Orbital binding energy in eV		
	DF	MCDF	Difference
1s	117219.54	117225.05	5.51
2s	22701.93	22705.93	4.01
2p <sub>1/2</sub>	21894.26	21897.37	3.11
2p <sub>3/2</sub>	18059.10	18063.37	4.27
3s	6367.67	6371.33	3.66
3p <sub>1/2</sub>	6002.20	6004.80	2.61
3p <sub>3/2</sub>	5106.02	5110.01	3.99
3d <sub>3/2</sub>	4530.82	4534.19	3.37
3d <sub>5/2</sub>	4350.02	4353.73	3.71
4s	2198.68	2202.10	3.42
4p <sub>1/2</sub>	2033.10	2034.68	1.58
4p <sub>3/2</sub>	1791.11	1795.03	3.92
4d <sub>3/2</sub>	1525.92	1528.51	2.60
4d <sub>5/2</sub>	1480.22	1483.63	3.41
4f <sub>5/2</sub>	1132.09	1134.94	2.85
4f <sub>7/2</sub>	1119.91	1123.20	3.29
5s	985.93	987.32	1.39
5p <sub>1/2</sub>	918.19	920.75	2.56

of the target atom. In the theoretical model, we consider the ionization of the projectile by the time varying field of the target atom as the projectile passes the target. However, projectile ionization by the electrons of the target atom is not considered, since its contribution to the total ionization cross sections scales only with  $Z_t$ , while the contribution of the target nucleus scales roughly with  $Z_t^2$  [4]. Furthermore, the effect of a target electron was shown to deviate from that of a target proton only near the ionization threshold [50].

Since the target potential is partially screened, it generates no asymptotic distortion and therefore the transition matrix as a function of the impact parameter  $\mathbf{b}$  corresponds to that of a first-order Born approximation:

$$\mathcal{A}_{if}(\mathbf{b}) = -i \int_{-\infty}^{+\infty} dt \phi_i(\mathbf{x}) \phi_f(\mathbf{x})^* V_t(s), \quad (3)$$

where  $\mathbf{x}$  and  $\mathbf{s} = \mathbf{x} - \mathbf{b} - \mathbf{v}_p t$  are the projectile active electron coordinates in the projectile and the target reference frame, respectively. The initial-bound (final-continuum) state of the projectile is  $\phi_i$  ( $\phi_f$ ), and  $V_t(s)$  is the short-range electrostatic interaction between the neutral target and the projectile active electron.

Typically, the application of first-order Born approximation, i.e., first-order perturbation theory, is justified for small Sommerfeld parameters,  $\nu = \sqrt{E_p^b/E_0} \ll 1$ . For the dominating ionization out of the  $4f^{14}$ -shell of  $\text{U}^{28+}$ , this is true since  $\nu = 0.26$  at 30 MeV/u and  $\nu = 0.20$  at 50 MeV/u.

The theoretical model used in the context of the current experiment exceeds the previous ones [45–47] in the application of fully relativistic bound-state wave functions for multielectron ions, which are required for a reliable description of cases

with a heavy projectile ion,  $Z_p \alpha \approx 1$  [4]. The radial parts of the initial-bound orbitals were provided by V. P. Shevelko [51] and calculated by means of the RICODE-M code as described in Ref. [52]. Later, the numerical radial wave functions were interpolated with a linear combination of Slater-type functions, and therefore each bound orbital has the expression

$$\phi_i(\mathbf{x}) = \sum_q C_q x^{n_q-1} \exp(-\alpha_q x) Y_l^m(\hat{\mathbf{x}}), \quad (4)$$

where the parameters  $C_q$ ,  $n_q$ , and  $\alpha_q$  arise from the interpolation, and  $Y_l^m$  are the spherical harmonics. The projectile final-continuum state,  $\phi_f(\mathbf{x})$ , is chosen as a hydrogenic continuum state with an effective charge given by the prescription of Belkić *et al.* [53],  $Z_{\text{eff}} = \sqrt{n^2 E_p^b / R_y}$ , with the principal quantum number of the initial-bound orbital  $n$  and the Rydberg energy  $R_y$ :

$$\phi_f(\mathbf{x}) = \frac{\exp(i \mathbf{p}' \cdot \mathbf{x})}{(2\pi)^{3/2}} N(\lambda) {}_1F_1[-i\lambda, 1, -i(p'x + \mathbf{p}' \cdot \mathbf{x})]. \quad (5)$$

Here,  $\mathbf{p}'$  is the ejected electron momentum in the projectile-fixed reference frame,  $\lambda = Z_{\text{eff}}/p'$ ,  ${}_1F_1$  the confluent hypergeometric function, and  $N(\lambda) = \exp(\lambda\pi/2)\Gamma(1+i\lambda)$  its corresponding normalization factor.

The ground-state configuration of  $\text{U}^{28+}$  is  $[\text{Kr}]4d^{10}4f^{14}5s^25p^2$ . For each subshell,  $E_p^b$  has been calculated using relativistic multiconfiguration Dirac-Fock (MCDHF) theory [49], as shown in Table I. From the listed fine structure levels, the weighted average of the binding energies of the individual  $nl$ -shells over the  $j = l \pm 1/2$  substates was used. The binding energies,  $E_p^b$ , thus determine the normalization of the transition matrix given in Eq. (3).

The potential  $V_t(s)$  of the target atom is approximated by an analytical two-parameter Green-Sellin-Zachor (GSZ) potential [54–56]. For the case of a neutral atom it reads

$$V_t(s) = -\frac{Z_t}{s} [H(e^{s/d} - 1) + 1]^{-1}. \quad (6)$$

The values applied for the parameters,  $H$  and  $d$ , are listed in Table II. Within the present theoretical model, these parameters determine the variation of the shape of the electron distribution for different  $Z_t$ .

In the target frame, the minimum momentum transfer of the target nucleus onto the projectile electron required for the ionization process is given by  $q_{\text{min}} = (E_p^b + E_e')/\gamma v_p$ , where  $E_e'$  is the kinetic energy of the emitted electron in the projectile frame [19]. The dominating impact parameter is then given by  $b \approx 1/q_{\text{min}} \approx 1$  a.u. for the studied collision systems. At these impact parameters there is a substantial screening effect according to the GSZ parameters given in Table II. Using these values, e.g., for the N target, the depth of the target potential is

reduced to one half of the pure Coulomb potential at a distance of 0.4 a.u. This is to be compared, e.g., with the collision system  $\text{U}^{88+} + \text{N}_2$  at 90 MeV/u, studied in Ref. [19], where  $b \approx 0.05$  a.u., such that the target screening is not relevant.

Electron-loss double-differential cross sections,  $d^2\sigma/dE_e'd\Omega_e'$ , are calculated as a function of the kinetic energy,  $E_e'(\mathbf{p}')$ , and the emission angle,  $\vartheta_e' = \angle(\mathbf{p}', \mathbf{v}_p)$ , in the primed projectile-fixed reference frame, and then transformed to the unprimed laboratory frame. Furthermore, an integration over the finite angular acceptance of the spectrometer is performed [19]:

$$\left. \frac{d^2\sigma}{dE_e'd\Omega_e'} \right|_{\vartheta_e=0^\circ} = \frac{1}{1 - \cos \vartheta_{\text{max}}} \int_0^{\vartheta_{\text{max}}} \frac{d^2\sigma}{dE_e'd\Omega_e'} \sin \vartheta_e' d\vartheta_e'. \quad (7)$$

The corresponding transformations of the electron energy and angle are given in Refs. [19,20].

## V. RESULTS AND DISCUSSION

In Fig. 1, the experimental results normalized to the theoretical calculations are given. The experimental results show a significant asymmetry in the cusp shape, which increases with the target atomic number  $Z_t$ . The asymmetry points to a strongly anisotropic electron emission in the projectile frame. This behavior is not reproduced by theory, which itself predicts a more symmetric cusp shape with only a weak dependence on  $Z_t$ .

In the evaluation of the measured electron energy distributions, no coincidence condition with the up-charged projectile ion was used (cf. Sec. III). Consequently, the electron distribution may not only contain contributions of ELC, but also of ECC, i.e., electrons from the target atom captured into the continuum of the projectile ion. However, even for the extreme case of a Xe target, further calculations performed within this study showed that the cross section for ECC is more than two orders of magnitude smaller than the cross section for ELC, thus being not relevant within the experimental accuracy.

The observed discrepancies do not change gradually across the electron energy, consequently they cannot be explained from the experimental side by a varying detection efficiency of the electron spectrometer across the studied electron energy range. Also, there is no obvious reason why the detection efficiency should change abruptly at the cusp energy,  $E_0$ . The similarity in the electron spectra of Figs. 1(a) and 1(b) measured at different projectile energies yields further confidence in the experimental data.

The applied theoretical model considers the ionization of the projectile ion by the screened potential of the target atom. However, the fact that the target atom is simultaneously ionized by the projectile ion is not considered in the present theory. The charge-state distributions of the ionized target atoms were studied for comparable collision systems in Refs. [57–59]. In an intuitive picture the ionization of the target atom causes a considerable change in the shape of the screened target potential, in the extreme case changing it into a pure Coulomb potential. An improved model could include two different target potentials, one for the incoming and one for the outgoing half-trajectory of the projectile ion, which might explain the observed cusp asymmetry.

TABLE II. GSZ parameters (in a.u.) for the H, N, and Xe targets; see Eq. (6).

Target	$Z_t$	$H$	$d$
H	1	0.824	1.107
N	7	2.340	1.170
Xe	54	6.513	1.259

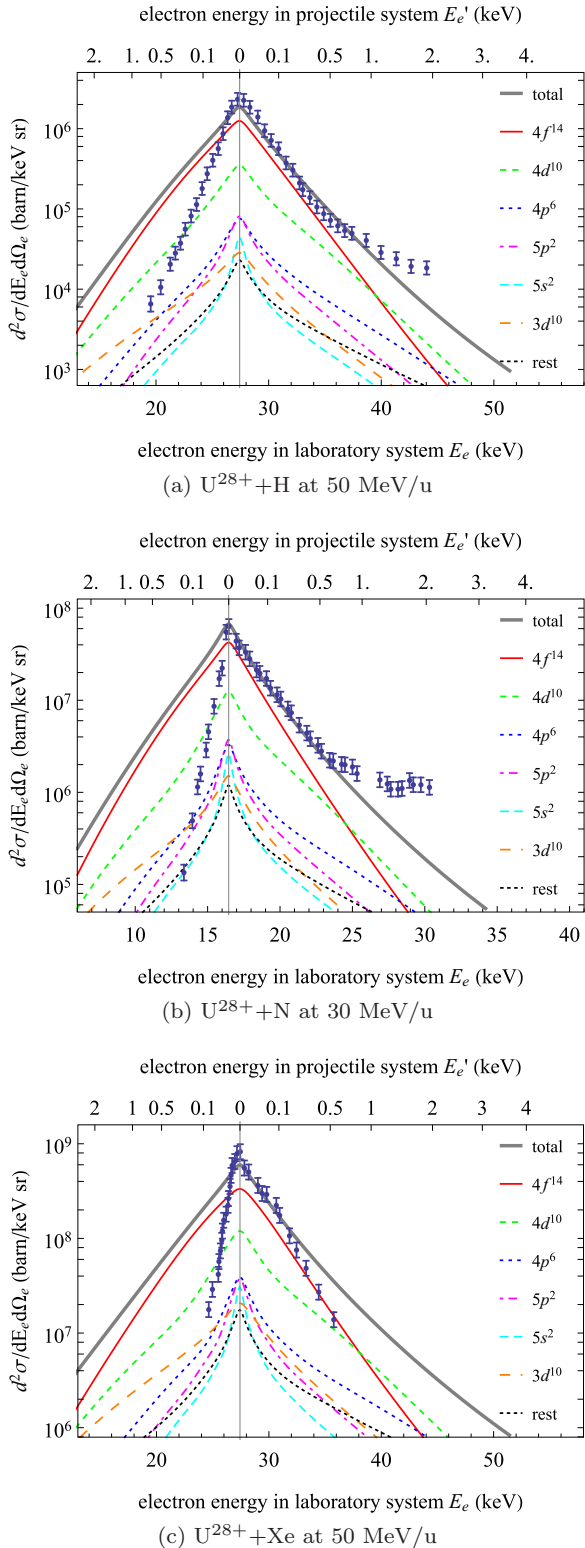


FIG. 1. Energy distribution of electrons observed within an angle of  $\vartheta_e = 0^\circ - 2.4^\circ$  with respect to the projectile beam in collisions of  $U^{28+}$  ions with gaseous targets. The experimental data (dots) were normalized to theory (lines). The contributions of the individual subshells of  $U^{28+}$  are shown. The lines labeled “rest” contain the contributions from the shells  $1s^2$ ,  $2s^2$ ,  $2p^6$ ,  $3s^2$ ,  $3p^6$ , and  $4s^2$ .

From the theoretical point of view, improvements to achieve better agreement could also arise from considering a two-step process in which the projectile electron is ionized by an interaction with the target nucleus and then interacts with its electronic cloud. This would be noticeable though only for small projectile frame energies, i.e., near the cusp maximum. Furthermore, a numerical distortion could be considered, instead of the asymptotic one, to describe the interaction between the projectile electron and the neutral target. Both of these improvements will be treated in the future.

The role of multiple ionization of  $U^{28+}$  ions in collisions with neutral targets was studied, e.g., in Refs. [30–33,35]. Multiple ionization of the projectile may occur either directly by the target atom or via inner-shell ionization with subsequent emission of an Auger electron. The experimental setup did not allow us to identify multiple ionization events. Cases of inner-shell ionization are included in the experimental data as well as in the theoretical model. These spectra are independent of whether an Auger electron is subsequently emitted or not. For  $U^{28+}$ , an Auger electron may be emitted after excitation or ionization of an inner-shell electron with a sufficiently strong binding energy. Estimates based on the binding energies of Table I show that an Auger effect with emission of an electron, e.g., from the  $5s$  or the  $5p$  shell, can only occur for an inner-shell vacancy in the  $4p$  shell, the  $4s$  shell, or any other shell of stronger binding energy. The probability of producing such an inner-shell vacancy in the considered collision systems is significantly smaller than the cross section for the ionization of a  $4f$  or  $4d$  electron, as can be seen in Fig. 1. In the projectile frame, Auger electrons are emitted with discrete energies, such that in the laboratory frame they appear as sharp lines at energies located symmetrically around the electron cusp [13–17]. Due to the comparably small cross sections for the required inner-shell excitation or ionization of the projectile, no Auger electrons were expected to be observed. However, the experimental data may include events of direct multiple ionization, where one of the ionized electrons was detected in the spectrometer. Part of the deviation between experimental data and theory might be attributed to the fact, that direct multiple ionization was not included in the theoretical model.

## VI. SUMMARY AND OUTLOOK

The presented experimental results for the electron-loss-to-continuum cusp of the multielectron projectiles  $U^{28+}$  in collisions with different neutral targets show a significant and varying cusp asymmetry. In contrast, the theoretical results based on relativistic first-order calculations show negligible dependence of the cusp shape on the target atomic number. This observation calls for further systematic study, which aims to separate effects of multielectron projectiles and effects of heavy neutral targets. Comparable impact parameters would be relevant, e.g., for  $K$ -shell ionization of  $Ar^{17+}$  by atomic targets at a projectile energy of 400 MeV/u. In these collision systems, effects of heavy-target screening on the electron emission spectra could be studied for a hydrogen-like projectile with the existing experimental setup at the ESR [4, Sec. 8.9].

## ACKNOWLEDGMENTS

This work was supported by Helmholtz International Center for FAIR through HGS-HIRE and the Helmholtz-CAS Joint Research Group HCJRG-108. R.D.R. and J.M.M. acknowledge support from the Agencia Nacional de Promoción Científica y Tecnológica of Argentina through Project No.

PICT 2011-2145. C.B. acknowledges support by Bundesministerium für Bildung und Forschung (Contracts No. 06GI911I, No. 05P12R6FAN, and No. 05P15RGFAA). The authors thank V. P. Shevelko for providing the wave functions for the  $U^{28+}$  orbitals and Z. W. Wu for performing the MCDF calculations for the orbital binding energies of  $U^{28+}$ .

- 
- [1] J. Briggs and J. Macek, *Adv. At. Mol. Opt. Phys.* **28**, 1 (1990).
- [2] N. Stolterfoht, R. D. DuBois, and R. D. Rivarola, *Electron Emission in Heavy Ion-Atom Collisions*, Springer Series on Atomic, Optical, and Plasma Physics, Vol. 20 (Springer, Berlin, 1997).
- [3] J. Ullrich and V. Shevelko, *Many-Particle Quantum Dynamics in Atomic and Molecular Fragmentation*, Springer Series on Atomic, Optical, and Plasma Physics, Vol. 35 (Springer, Berlin, 2003).
- [4] A. Voitkiv and J. Ullrich, *Relativistic Collisions of Structured Atomic Particles*, Springer Series on Atomic, Optical, and Plasma Physics, Vol. 49 (Springer, Berlin, 2008).
- [5] V. Shevelko and H. Tawara, *Atomic Processes in Basic and Applied Physics*, Springer Series on Atomic, Optical, and Plasma Physics, Vol. 68 (Springer, Berlin, 2012).
- [6] A. B. Voitkiv, B. Najjari, and J. Ullrich, *Phys. Rev. A* **76**, 022709 (2007).
- [7] J. S. Briggs, in *Quantum Electrodynamics of Strong Fields*, edited by W. Greiner (Springer US, Boston, MA, 1983), p. 521.
- [8] U. Thumm, J. S. Briggs, and O. Scholler, *J. Phys. B* **21**, 833 (1988).
- [9] D. H. Jakubassa-Amundsen, *J. Phys. B* **26**, L227 (1993).
- [10] N. Stolterfoht, D. Schneider, D. Burch, H. Wieman, and J. Risley, *Phys. Rev. Lett.* **33**, 59 (1974).
- [11] M. Breinig, S. B. Elston, S. Hultdt, L. Liljeby, C. R. Vane, S. D. Berry, G. A. Glass, M. Schauer, I. A. Sellin, G. D. Alton, S. Datz, S. Overbury, R. Laubert, and M. Suter, *Phys. Rev. A* **25**, 3015 (1982).
- [12] K. F. Man, W. Steckelmacher, and M. W. Lucas, *J. Phys. B* **19**, 401 (1986).
- [13] L. H. Andersen, M. Frost, P. Hvelplund, H. Knudsen, and S. Datz, *Phys. Rev. Lett.* **52**, 518 (1984).
- [14] L. H. Andersen, M. Frost, P. Hvelplund, and H. Knudsen, *J. Phys. B* **17**, 4701 (1984).
- [15] D. Schneider, G. Schiwietz, and D. DeWitt, *Phys. Rev. A* **47**, 3945 (1993).
- [16] S. Datz, R. Hippler, L. H. Andersen, P. F. Dittner, H. Knudsen, H. F. Krause, P. D. Miller, P. L. Pepmiller, T. Rosseel, R. Schuch, N. Stolterfoht, Y. Yamazaki, and C. R. Vane, *Phys. Rev. A* **41**, 3559 (1990).
- [17] C. Liao, S. Hagmann, T. Zouros, E. Montenegro, G. Toth, P. Richard, S. Grabbe, and C. Bhalla, *Nucl. Instrum. Methods B* **98**, 324 (1995).
- [18] B. Najjari, A. Surzhykov, and A. B. Voitkiv, *Phys. Rev. A* **77**, 042714 (2008).
- [19] P.-M. Hillenbrand, S. Hagmann, A. B. Voitkiv, B. Najjari, D. Banaś, K.-H. Blumenhagen, C. Brandau, W. Chen, E. De Filippo, A. Gumberidze, D. L. Guo, C. Kozhuharov, M. Lestinsky, Y. A. Litvinov, A. Müller, H. Rothard, S. Schippers, M. S. Schöffler, U. Spillmann, S. Trotsenko, X. L. Zhu, and T. Stöhlker, *Phys. Rev. A* **90**, 042713 (2014).
- [20] P.-M. Hillenbrand, S. Hagmann, D. Atanasov, D. Banaś, K.-H. Blumenhagen, C. Brandau, W. Chen, E. De Filippo, A. Gumberidze, D. L. Guo, D. H. Jakubassa-Amundsen, O. Kovtun, C. Kozhuharov, M. Lestinsky, Y. A. Litvinov, A. Müller, R. A. Müller, H. Rothard, S. Schippers, M. S. Schöffler, U. Spillmann, A. Surzhykov, S. Trotsenko, N. Winckler, X. L. Yan, V. A. Yerokhin, X. L. Zhu, and T. Stöhlker, *Phys. Rev. A* **90**, 022707 (2014).
- [21] P.-M. Hillenbrand, S. Hagmann, D. H. Jakubassa-Amundsen, J. M. Monti, D. Banaś, K.-H. Blumenhagen, C. Brandau, W. Chen, P. D. Fainstein, E. De Filippo, A. Gumberidze, D. L. Guo, M. Lestinsky, Y. A. Litvinov, A. Müller, R. D. Rivarola, H. Rothard, S. Schippers, M. S. Schöffler, U. Spillmann, S. Trotsenko, X. L. Zhu, and T. Stöhlker, *Phys. Rev. A* **91**, 022705 (2015).
- [22] P.-M. Hillenbrand, S. Hagmann, Y. A. Litvinov, and T. Stöhlker, *J. Phys. Conf. Ser.* **635**, 012011 (2015).
- [23] H.-P. Hülskötter, B. Feinberg, W. E. Meyerhof, A. Belkacem, J. R. Alonso, L. Blumenfeld, E. A. Dillard, H. Gould, N. Guardala, G. F. Krebs, M. A. McMahan, M. E. Rhoades-Brown, B. S. Rude, J. Schweppe, D. W. Spooner, K. Street, P. Thieberger, and H. E. Wegner, *Phys. Rev. A* **44**, 1712 (1991).
- [24] R. D. DuBois, A. C. F. Santos, G. M. Sigaud, and E. C. Montenegro, *Phys. Rev. A* **84**, 022702 (2011).
- [25] G. Weber, C. Omet, R. D. DuBois, O. de Lucio, T. Stöhlker, C. Brandau, A. Gumberidze, S. Hagmann, S. Hess, C. Kozhuharov, R. Reuschl, P. Spiller, U. Spillmann, M. Steck, M. Thomason, and S. Trotsenko, *Phys. Rev. ST Accel. Beams* **12**, 084201 (2009).
- [26] G. Weber, M. O. Herdrich, R. D. DuBois, P.-M. Hillenbrand, H. Beyer, L. Bozyk, T. Gassner, R. E. Grisenti, S. Hagmann, Y. A. Litvinov, F. Nolden, N. Petridis, M. S. Sanjari, D. F. A. Winters, and T. Stöhlker, *Phys. Rev. ST Accel. Beams* **18**, 034403 (2015).
- [27] G. Baur, I. L. Beigman, V. P. Shevelko, I. Y. Tolstikhina, and T. Stöhlker, *Phys. Rev. A* **80**, 012713 (2009).
- [28] V. Shevelko, I. Beigman, M. Litsarev, H. Tawara, I. Tolstikhina, and G. Weber, *Nucl. Instrum. Methods B* **269**, 1455 (2011).
- [29] V. Shevelko, M.-Y. Song, I. Tolstikhina, H. Tawara, and J.-S. Yoon, *Nucl. Instrum. Methods B* **278**, 63 (2012).
- [30] W. E. Meyerhof, R. Anholt, X.-Y. Xu, H. Gould, B. Feinberg, R. J. McDonald, H. E. Wegner, and P. Thieberger, *Phys. Rev. A* **35**, 1967 (1987).
- [31] R. Anholt, W. E. Meyerhof, X.-Y. Xu, H. Gould, B. Feinberg, R. J. McDonald, H. E. Wegner, and P. Thieberger, *Phys. Rev. A* **36**, 1586 (1987).
- [32] R. E. Olson, R. L. Watson, V. Horvat, A. N. Perumal, Y. Peng, and T. Stöhlker, *J. Phys. B* **37**, 4539 (2004).

- [33] R. D. DuBois, A. C. F. Santos, T. Stöhlker, F. Bosch, A. Bräuning-Demian, A. Gumberidze, S. Hagmann, C. Kozhuharov, R. Mann, A. O. Muthig, U. Spillmann, S. Tachenov, W. Bart, L. Dahl, B. Franzke, J. Glatz, L. Gröning, S. Richter, D. Wilms, K. Ullmann, and O. Jagutzki, *Phys. Rev. A* **70**, 032712 (2004).
- [34] V. I. Matveev, D. U. Matrasulov, and S. V. Ryabchenko, *J. Exp. Theor. Phys.* **102**, 1 (2006).
- [35] M.-Y. Song, M. Litsarev, V. Shevelko, H. Tawara, and J.-S. Yoon, *Nucl. Instrum. Methods B* **267**, 2369 (2009).
- [36] C. Omet, P. Spiller, J. Stadlmann, and D. H. H. Hoffmann, *New J. Phys.* **8**, 284 (2006).
- [37] E. Mahner, *Phys. Rev. ST Accel. Beams* **11**, 104801 (2008).
- [38] L. Bozyk, F. Chill, M. Litsarev, I. Tolstikhina, and V. Shevelko, *Nucl. Instrum. Methods B* **372**, 102 (2016).
- [39] R. D. DuBois, O. de Lucio, M. Thomason, G. Weber, T. Stöhlker, K. Beckert, P. Beller, F. Bosch, C. Brandau, A. Gumberidze, S. Hagmann, C. Kozhuharov, F. Nolden, R. Reuschl, J. Rzadkiewicz, P. Spiller, U. Spillmann, M. Steck, and S. Trotsenko, *Nucl. Instrum. Methods B* **261**, 230 (2007).
- [40] O. Uwira, A. Müller, W. Spies, A. Frank, J. Linkemann, L. Empacher, P. Mokler, R. Becker, M. Kleinod, and S. Ricz, *Nucl. Instrum. Methods B* **98**, 162 (1995).
- [41] D. M. Mitnik, M. S. Pindzola, F. Robicheaux, N. R. Badnell, O. Uwira, A. Müller, A. Frank, J. Linkemann, W. Spies, N. Angert, P. H. Mokler, R. Becker, M. Kleinod, S. Ricz, and L. Empacher, *Phys. Rev. A* **57**, 4365 (1998).
- [42] W. Barth, A. Adonin, C. E. Düllmann, M. Heilmann, R. Hollinger, E. Jäger, J. Khuyagbaatar, J. Krier, P. Scharrer, H. Vormann, and A. Yakushev, *Phys. Rev. ST Accel. Beams* **18**, 040101 (2015).
- [43] N. Petridis, The Internal Multiphase Target for Storage Ring Experiments, Ph.D. thesis, Goethe-Universität, Frankfurt, 2014.
- [44] Strictly speaking, the maximum of the electron cusp is at  $E_0$  only for a symmetric cusp shape, while for a very pronounced forward-backward asymmetry of the electron distribution, the maximum of the cusp is slightly shifted (see, e.g., Refs. [20,21]). However, this effect is not significant within the experimental accuracy of the present data.
- [45] J. M. Monti, R. D. Rivarola, and P. D. Fainstein, *J. Phys. B* **41**, 201001 (2008).
- [46] J. M. Monti, R. D. Rivarola, and P. D. Fainstein, *J. Phys. B* **44**, 195206 (2011).
- [47] D. Fregenal, J. M. Monti, J. Fiol, P. D. Fainstein, R. D. Rivarola, G. Bernardi, and S. Suárez, *J. Phys. B* **47**, 155204 (2014).
- [48] K. Rashid, M. Saadi, and M. Yasin, *At. Data Nucl. Data Tables* **40**, 365 (1988).
- [49] F. Parpia, C. Fischer, and I. Grant, *Comput. Phys. Commun.* **94**, 249 (1996).
- [50] B. Najjari and A. B. Voitkiv, *Phys. Rev. A* **87**, 034701 (2013).
- [51] V. P. Shevelko (private communication, 2015).
- [52] I. Yu. Tolstikhina, I. I. Tupitsyn, S. N. Andreev, and V. P. Shevelko, *J. Exp. Theor. Phys.* **119**, 1 (2014).
- [53] D. Belkic, *Phys. Rep.* **56**, 279 (1979).
- [54] A. Green, D. Sellin, and A. Zachor, *Phys. Rev.* **184**, 1 (1969).
- [55] P. Szydlak and A. Green, *Phys. Rev. A* **9**, 1885 (1974).
- [56] R. Garvey, C. Jackman, and A. Green, *Phys. Rev. A* **12**, 1144 (1975).
- [57] S. Kelbch, J. Ullrich, R. Mann, P. Richard, and H. Schmidt-Böcking, *J. Phys. B* **18**, 323 (1985).
- [58] H. Berg, R. Dörner, C. Kelbch, S. Kelbch, J. Ullrich, S. Hagmann, P. Richard, H. Schmidt-Böcking, A. S. Schlachter, M. Prior, H. J. Crawford, J. M. Engelage, I. Flores, D. H. Loyd, J. Pedersen, and R. E. Olson, *J. Phys. B* **21**, 3929 (1988).
- [59] S. Kelbch, C. L. Cocke, S. Hagmann, M. Horbatsch, C. Kelbch, R. Koch, H. Schmidt-Böcking, and J. Ullrich, *J. Phys. B* **23**, 1277 (1990).